Transformation and crystallization energetics of synthetic and biogenic amorphous calcium carbonate

A. V. Radha[a], Tori Z. Forbes[a], Christopher E. Killian[b], P. U. P. A. Gilbert[b,2], and Alexandra Navrotsky[a,1]

[a]Peter A. Rock Thermochemistry Laboratory and Nanomaterials in the Environment, Agriculture, and Technology Organized Research Unit (NEAT ORU), University of California at Davis, One Shields Avenue, Davis, CA 95616; and [b]Department of Physics, University of Wisconsin at Madison, 1150 University Avenue, Madison, WI 53706

Contributed by Alexandra Navrotsky, July 24, 2010 (sent for review January 19, 2010)

Amorphous calcium carbonate (ACC) is a metastable phase often observed during low temperature inorganic synthesis and biomineralization. ACC transforms with aging or heating into a less hydrated form, and with time crystallizes to calcite or aragonite. The energetics of transformation and crystallization of synthetic and biogenic (extracted from California purple sea urchin larval spicules, *Strongylocentrotus purpuratus*) ACC were studied using isothermal acid solution calorimetry and differential scanning calorimetry. Transformation and crystallization of ACC can follow an energetically downhill sequence: more metastable hydrated ACC → less metastable hydrated ACC ⇒ anhydrous ACC ~ biogenic anhydrous ACC ⇒ vaterite → aragonite → calcite. In a given reaction sequence, not all these phases need to occur. The transformations involve a series of ordering, dehydration, and crystallization processes, each lowering the enthalpy (and free energy) of the system, with crystallization of the dehydrated amorphous material lowering the enthalpy the most. ACC is much more metastable with respect to calcite than the crystalline polymorphs vaterite or aragonite. The anhydrous ACC is less metastable than the hydrated, implying that the structural reorganization during dehydration is exothermic and irreversible. Dehydrated synthetic and anhydrous biogenic ACC are similar in enthalpy. The transformation sequence observed in biomineralization could be mainly energetically driven; the first phase deposited is hydrated ACC, which then converts to anhydrous ACC, and finally crystallizes to calcite. The initial formation of ACC may be a first step in the precipitation of calcite under a wide variety of conditions, including geological CO_2 sequestration.

amorphous calcium carbonate (ACC) | calorimetry | crystallization enthalpy | sea urchin larval spicules | synthetic and biogenic ACC

Calcium carbonate is ubiquitous in nature and found in fresh and saline waters, soils, sediments, mineral dusts, and geologic formations (1–3). Calcium carbonate occurs in five different crystalline polymorphs at ambient pressure, anhydrous phases (calcite, aragonite, and vaterite), and hydrated phases (monohydrocalcite $CaCO_3{\cdot}H_2O$ and ikaite $CaCO_3{\cdot}6\,H_2O$), and various amorphous forms as well (1, 3). Amorphous calcium carbonate (ACC) is transient and transforms into one of the crystalline forms in presence of water or when heated.

ACC can form by both biological and abiotic means. In organisms as diverse as mollusks, sea urchins, sponges, ascidians/sea squirts, and crustaceans, ACC is a precursor to complex calcite and aragonite structures in shells, spines, teeth, and spicules (3–12). Abiotically, ACC is easily formed by mixing aqueous solutions at or below room temperature. These solutions can be totally inorganic or they can contain small organic species which affect the formation and persistence of ACC (13–20). Increasing interest in CO_2 sequestration has led to proposals and pilot projects in which large plumes of supercritical carbon dioxide would be introduced into deep saline aquifers (21–25). ACC may be produced as an initial reaction product between the CO_2 and the aqueous phase, with mineral surfaces and small pores acting as possible nucleation sites (26).

The ACC formed by these various processes is a variable and still poorly understood material. Two forms, anhydrous transient ACC and a hydrated ACC containing about 1 mol of water that persists for longer time periods exist in biogenic sources (4, 9, 10, 27). The chemically precipitated ACC is also variable in particle size and water content and transforms to a less hydrated or anhydrous form upon heating before crystallization sets in (18, 19, 28). A central question, which the present work addresses, is the nature of the compositional, structural, and energetic similarities and differences among different ACC samples (both chemically and biologically produced) and their transformations with heating.

Several computational and experimental studies on formation mechanism and structural characteristics of ACC have recently appeared. A metadynamics study including computation of free energy suggests preference for an amorphous structure during the early stages of crystal growth (29). Molecular dynamics studies indicate that the initial binding of calcium to carbonate and subsequent growth of amorphous clusters in water is not only energetically favorable, but also virtually free from thermodynamic barriers (30). Nuclear magnetic resonance, X-ray absorption spectroscopy, and infrared spectroscopy have studied the structure of ACC (3, 7, 31, 32). High-energy X-ray total scattering studies on ACC indicate no structural coherence beyond 1.5 nm distance (20).

Soluble clusters have been found in solution prior to the nucleation of calcium carbonate, such clusters are similar in size to the structural coherence length of ACC. Based on equilibrium thermodynamics, Gebauer et al. (33) demonstrated qualitatively the formation of stable ~2 nm clusters prior to nucleation. Pouget et al. observed the initial formation of 0.6 to 1.1 nm prenucleation clusters using cryogenic transmission electron microscopy (34). On aggregation, these clusters lead to the formation of ACC nanoparticles approximately 30 nm in diameter. These observations suggest a new and more complex pathway for calcium carbonate formation through stable nanoscopic prenucleation clusters as opposed to the simple picture provided by classical nucleation theory (35, 36).

If prenucleation clusters, ACC, and nano-calcite are often encountered in the initial stages of calcite precipitation from aqueous solutions, then these materials and their transformations could be important in a broad environmental, biological, and technological context. To understand the role of ACC in biomineralization, CO_2 sequestration, carbonate rock formation, and other processes, the energetics of this system must be character-

Author contributions: A.V.R. and A.N. designed research; A.V.R., T.Z.F., and C.E.K. performed research; C.E.K., P.U.P.A.G., and A.N. contributed new reagents/analytic tools; A.V.R., T.Z.F., P.U.P.A.G., and A.N. analyzed data; and A.V.R., T.Z.F., P.U.P.A.G., and A.N. wrote the paper.

The authors declare no conflict of interest.

[1]To whom correspondence should be addressed. E-mail: anavrotsky@ucdavis.edu.

[2]Previously publishing as Gelsomina De Stasio.

This article contains supporting information online at www.pnas.org/lookup/suppl/doi:10.1073/pnas.1009959107/-/DCSupplemental.

ized. A study by Wan et al. investigated the dynamic process of calcium carbonate precipitation with different amounts of L-aspartic acid by microcalorimetry (37). Wan et al. observed two calorimetric peaks corresponding to formation of a transient ACC and its transformation to a crystalline phase. In addition, there are three reports of thermally induced crystallization of ACC to calcite at approximately 320 °C using differential scanning calorimetry (DSC) (18, 19, 38).

The present study investigates the enthalpies of transformation and crystallization in synthetic and biogenic ACC to provide a comprehensive picture of their relative stabilities. Synthetic ACC samples were freshly prepared in our laboratory without the use of organic additives and biogenic-ACC samples were extracted from California purple sea urchin (*S. purpuratus*) larval spicules. The transformation of hydrous synthetic and biogenic ACC to calcite at ambient temperature was measured using acid solution calorimetry. The dehydration of hydrous ACC, followed by the crystallization of anhydrous ACC to calcite on heating, was analyzed using DSC. This study provides information on the metastability, dehydration, and crystallization energetics, and a possible crystallization pathway for ACC. This study also includes the direct measurement of crystallization enthalpy of biogenic ACC. Major findings are that ACC is a highly metastable phase compared to all crystalline $CaCO_3$ polymorphs, that the dehydrated ACC produced by heating the chemically precipitated phase is energetically similar to biogenic ACC, and that the sequence of transformations, more metastable hydrated ACC—less metastable hydrated ACC—anhydrous ACC ~ biogenic anhydrous ACC—vaterite—aragonite—calcite, provides an energetically downhill reaction pathway for crystallization.

Results

The absence of a crystalline phase in ACC samples was confirmed by X-ray diffraction (XRD) and Fourier Transform Infrared (FTIR) spectroscopy. The water content was estimated from the first weight loss step (ambient to 200 °C) in the themogravimetric analysis (TGA) curve. The thermal behavior of ACC on heating was studied using DSC. Enthalpies of solution at ambient conditions were done using isothermal acid solution calorimetry. The *Materials and Methods* section below and the deposited *SI Text* provide details.

Synthetic ACC. To minimize the crystallization of initial materials, we studied five freshly prepared ACC samples (ACC-1 to 5) synthesized under similar conditions. All these samples are hydrated with composition $CaCO_3 \cdot n\,H_2O$. The absence of any Bragg reflections in the powder XRD patterns indicates the formation of an amorphous phase (Fig. 1). Two diffuse maxima centered at 20 and 45° 2θ are common features for the ACC phase and were

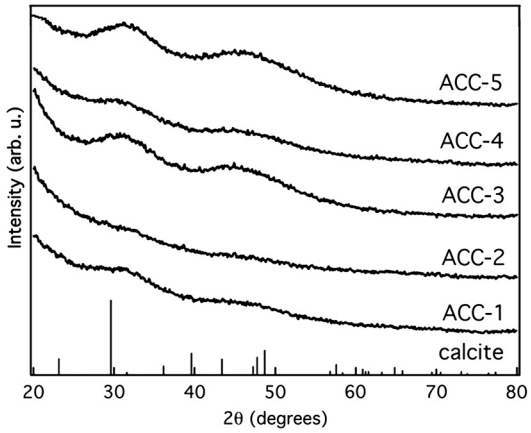

Fig. 1. Powder XRD patterns of more disordered (ACC-1 and -2), less disordered (ACC-3 to 5) synthetic ACC, and calcite PDF: 60-7239.

previously observed (19, 20). The variable temperature powder XRD patterns of the synthetic ACC-1, 4, and 5 samples indicate that ACC persists up to 330 °C (see Fig. S1) and crystallization to calcite occurs above this temperature.

The FTIR spectra of synthetic ACC are shown in Fig. S2*A*. The absence of the sharp ν_4 band at 713 cm^{-1} in the FTIR spectra indicate the absence of significant amounts of calcite in these samples (Table 1 and Figs. S2*A*, S3*A*). The O-H stretching vibration around 3,400 cm^{-1} indicates the presence of water in the samples. The water content ranges from 1.20 to 1.58 moles H_2O per mole $CaCO_3$, which is consistent with the hydration state of persistent ACC (Fig. S4).

Both SEM and surface area measurement by the Brunauer-Emmett-Teller (BET) method were used to estimate the particle size of the synthetic ACC (Table 1). The observed particle size in the SEM images ranges from 50 to 200 nm, whereas BET analysis indicates particle sizes between 80 to 400 nm. Considering the uncertainties, the two sets of data are in reasonable agreement. We have some evidence that the ACC may have dehydrated and crystallized in the high vacuum of the SEM, but the main purpose of SEM was to check particle size, which should not have been affected.

The enthalpies of solution in 5 N HCl (ΔH_{sln}) range from -46.3 ± 0.9 to -53.3 ± 1.4 kJ/mol (Table 2). The enthalpy of solution of calcite (Fisher Chemicals) is -28.8 ± 0.3 kJ/mol. The solution enthalpy values for ACC samples are more exothermic than that of calcite (Table 2). Using these values in a thermochemical cycle (see *SI Text: Thermochemical cycle-1*), we calculated the enthalpies for the crystallization (ΔH_{cryst}) of the hydrous ACC phase to the stable calcite phase at 26 °C. These vary from -17 ± 1 to -24 ± 1 kJ/mol for the synthetic ACC samples (Table 2) and do not show any correlation with either water content or surface area (Fig. S5). This variation may be caused by small differences in preparation conditions (mixing, filtration, or aging during storage). Broadly, the synthetic ACC samples fall into two distinct ranges of enthalpies of crystallization. The samples ACC-1 and ACC-2 show more exothermic crystallization enthalpies (-24 ± 1 kJ/mol) and the other samples, ACC-3, -4, and -5, show less exothermic values (-17 ± 1 kJ/mol).

The DSC curves (Fig. S4) exhibit two peaks. The first peak at 100 °C is endothermic and corresponds to dehydration of ACC. A rough integration of this DSC peak for different samples, normalized to the amount of water loss, gives a value close to the enthalpy of vaporization of liquid water at 100 °C (40.87 kJ/mol). The second sharp exotherm at 327 °C is due to the crystallization of the dehydrated synthetic ACC phase and agrees with the calcite crystallization temperature observed by variable temperature XRD. The enthalpies of crystallization of anhydrous synthetic ACC at 327 °C ($\Delta H_{ahhydACC\text{-}cryst}$ at T_{cryst}) were calculated from the second exothermic DSC peak (Table 2) and vary from -12.8 ± 0.5 to -15.4 ± 0.4 kJ/mol for different synthetic samples. Other thermodynamic studies of synthetic ACC by Koga and Yamane and Koga et al. reported wider variations in thermally induced enthalpies of crystallization (-13.1 ± 0.2 and -19.1 ± 0.2 kJ/mol (22); -12.3 ± 0.2 to -39.9 ± 2.1 kJ/mol (21)).

Biogenic ACC from Sea Urchin Larval Spicules. Several biogenic-ACC samples extracted from 72 h (spicule-72-1 and 72-2) and 48 h (spicule-48-1 to 48-6) sea urchin embryo spicules (California purple sea urchin, *S. purpuratus*) were studied within 1 d of extraction. Similarly extracted material has been reported to contain 5 mol% magnesium with the composition $Ca_{0.95}Mg_{0.05}CO_3 \cdot n\,H_2O$ (27). We confirmed this composition for the spicule samples by inductively coupled plasma mass spectrometry. The powder XRD patterns of the samples extracted after 48 h (spicule-48-1 to 48-4) show low intensity Bragg reflections corresponding to calcite. In contrast, the powder XRD patterns of the samples extracted

Table 1. Characterization of the synthetic ACC samples

Sample description					Particle size (nm)	
Type	ID	H_2O, n (mol) from TGA	FTIR $I(\nu_2)/I(\nu_4)$	BET surface area (m^2/g)	BET	SEM
Synthetic calcite	Calcite	0	1.4	0.99 ± 0.08	-	
More disordered synthetic ACC (more metastable)	ACC-1	1.20 ± 0.02	8.0	19.3 ± 0.2	192 ± 3	-
	ACC-2	1.58 ± 0.01	9.5	9.0 ± 1	412 ± 53	~200
Less disordered Synthetic ACC (less metastable)	ACC-3	1.46 ± 0.01	6.8	12.1 ± 0.2	306 ± 6	-
	ACC-4	1.36 ± 0.01	6.2	12.5 ± 0.1	296 ± 3	150–200
	ACC-5	1.13 ± 0.02	7.2	42.4 ± 0.2	86 ± 4	50–100

after 72 h show well defined Bragg reflections of calcite (see Fig. S6).

The FTIR spectra of spicules are shown in Fig. S2*B*. The FTIR spectra suggest spicules-72-1, and 72-2 have crystallized to calcite, whereas spicules-48-1 to 48-6 are mixed calcite and ACC phases (Table 3 and Figs. S2*B* and S3*B*). The well defined Bragg reflections in the XRD pattern and the absence of any "amorphous bump" in the diffraction pattern argue strongly that these samples are mostly calcite, with little ACC left (see Fig. S6). The measured enthalpies are consistent with mainly crystalline calcite in spicule-48-5 and 48-6 (Table 2). The low intensity broad O-H stretching vibration around 3,400 cm^{-1} indicates the presence of a small amount of water in these samples. The TGA studies indicate the spicule samples contain less water than synthetic ACC, namely 0.16–0.35 mol H_2O per formula unit (Table 3). Based on these measurements, we can classify spicule samples into two groups as biogenic ACC (spicule-48-1 to 48-4) and biogenic calcite (spicules-72-1, 72-2,-48-5, and 48-6).

The measured enthalpies of solution are summarized in Table 2. For biogenic calcite with 5 mol% Mg (spicules 72-1, 72-2, 48-5, and 48-6), the enthalpy of solution is -29.5 ± 0.6 kJ/mol (Table 2). The enthalpies of solution of spicule-48-4 and 48-5 confirm that these samples had crystallized to calcite since this enthalpy is very close to that of pure calcite (-28.8 ± 0.3 kJ/mol). For enthalpies of solution of hydrated phases at 26 °C ($\Delta H_{sln\text{-}spicule}$) at ambient conditions, the corrections for contributions of water have been made (*SI Text: Thermochemical cycle-2*). For the biogenic-ACC samples (spicule-48-1 to 48-3), which contained calcite impurities, a correction was also applied assuming the sample to be 90% biogenic ACC and 10% biogenic calcite (*SI Text: Thermochemical cycle-3*). The enthalpies of crystallization from biogenic ACC to biogenic calcite at 26 °C ($\Delta H_{cryst\text{-}bio}$) are then calculated using the corrected enthalpies of solution (*SI Text: Thermochemical cycle-4*). The enthalpy of crystallization at 26 °C ($\Delta H_{cryst\text{-}bio}$) from anhydrous biogenic ACC to biogenic calcite is -12.9 ± 0.8 kJ/mol. Applying the correction for 10% calcite in the biogenic ACC modifies the enthalpy of crystallization to -14.3 ± 1 kJ/mol. Unlike synthetic ACC, the biogenic-ACC spicules are almost anhydrous (0.25 mol of water), which crystallizes easily to calcite.

DSC measurements of the calcite spicules and synthetic calcite samples showed no exothermic crystallization peaks. The DSC results confirms that the spicules 72-1, 72-2, and 48-5 are crystalline calcite and do not contain significant residual ACC. The DSC on biogenic ACC (spicule-48-4) was carried out with a very small (~0.7 mg) sample and no peak could be resolved.

Discussion

Fig. 2 presents a stability diagram or energy landscape for the calcium carbonate system, including the crystalline and various amorphous phases. The stability expressed as the enthalpy relative to calcite likely also represents the order of free energy because the TΔS term is probably small at room temperature. The figure illustrates several important points. (*i*) An energetically downhill sequence can be inferred: more metastable hydrated ACC—less metastable hydrated ACC—anhydrous ACC~ biogenic anhydrous ACC—vaterite—aragonite—calcite. (*ii*) Hydrated and dehydrated ACC are much higher in enthalpy than any

Table 2. Calorimetric data

Sample description		Acid calorimetry in 5 N HCl, 26 °C		DSC	
Type	ID	ΔH_{sln} (kJ/mol)	ΔH_{cryst} at 26 °C (kJ/mol) (ACC to calcite)	T_{cryst} (°C)	$\Delta H_{anhydACC\text{-}cryst}$ at T_{cryst} (kJ/mol) * (anhydrous ACC to calcite)
Synthetic calcite	Calcite	−28.75 ± 0.26 (7)	-	-	-
More disordered synthetic ACC(more metastable)	ACC-1	−50.70 ± 1.78 (5)	−21.47 ± 1.80	326	−15.4 ± 0.4
	ACC-2	−53.33 ± 1.38 (3)	−23.95 ± 1.40	327	−13.3 ± 0.7
Less disordered Synthetic ACC (less metastable)	ACC-3	−46.33 ± 0.93 (4)	−17.00 ± 0.97	329	−15.2 ± 0.3
	ACC-4	−46.38 ± 0.60 (5)	−17.09 ± 0.65	327	−14.8 ± 0.9
	ACC-5	−46.81 ± 0.85(4)	−17.61 ± 0.89	313	−12.8 ± 0.5
ACC-spicules (biogenic ACC)	spicule-48-1 to 48-3	−42.50 ± 0.47 (3) (−43.84 ± 0.68) †	−12.86 ± 0.76 ‡ (−14.29 ± 0.97) ‡ †		
Calcite-spicules (biogenic calcite)	Spicule-72-1 and 72-2	−29.60 ± 0.60 (5) (−29.54 ± 0.60) §	-		
	spicule-48-5 and 48-6	−29.81 ± 0.48 (4) (−29.67 ± 0.48) §	-		

Extra decimal places are retained to prevent round-off error. Uncertainties are given as two standard deviations of the mean. Values in parentheses are the number of experiments. The symbols ΔH_{sln} and ΔH_{cryst} stand for the enthalpies of dissolution and crystallization respectively.

*Enthalpy of crystallization of anhydrous ACC to calcite ($\Delta H_{anhydACC\text{-}cryst}$) from exothermic DSC peak at crystallization temperature T_{cryst}.

†Values with 10% calcite and water corrections.

‡Enthalpy of crystallization of biogenic-ACC to biogenic-calcite ($\Delta H_{cryst\text{-}bio}$).

§Values with water correction ($\Delta H = -0.4$ kJ/mol (50)).

Table 3. Characterization of the spicule samples

Sample description		H_2O, *n* (moles)	$I(\nu_2)/I(\nu_4)$
Type	ID	from TGA	FTIR
ACC-spicules	Spicule-48-1	-	8.3
(biogenic ACC)	Spicule-48-2	-	-
	Spicule-48-3	-	3.3
	Spicule-48-4	0.25 ± 0.01	7.3
Calcite-spicules	Spicule-48-5	0.35 ± 0.01	7.2
(biogenic	Spicule-48-6	-	5.6
calcite)	Spicule-72-1	0.16 ± 0.02	2.3
	Spicule-72-2	0.16 ± 0.02	4.0

of the crystalline polymorphs, which are all similar in energy. This trend suggests that ACC is a suitable precursor for all $CaCO_3$ polymorphs, and which phases actually are formed in the transformation sequence above, and which are bypassed, can be kinetically controlled. (*iii*) The formation of anhydrous ACC from hydrated ACC is exothermic. Thus anhydrous ACC is less metastable than the hydrated material and its formation is a thermodynamically irreversible process. (*iv*) Dehydrated synthetic and biogenic ACC have similar enthalpies. (*v*) There appear to be two energetically distinct groups of hydrated synthetic ACC, more metastable and less metastable, see discussion below.

These data support previous studies (18, 19) indicating that ACC is indeed metastable with respect to any of the crystalline calcium carbonate phases. Both hydrated and dehydrated ACC are high-energy metastable phases and there is a big energetic driving force for their crystallization. This large energy difference between hydrated amorphous and dehydrated crystalline phases is similar to the energetics of amorphous oxides such as zirconia and silica (39, 40). The surface energies of the amorphous oxide materials are significantly smaller than those of their crystalline counterparts, suggesting that small particle size could lead to thermodynamic stabilization of amorphous relative to crystalline nanoscale materials (41, 42). The surface energies of amorphous and crystalline calcium carbonates are currently unknown, but may also affect the energetics of the system.

The formation of anhydrous ACC from the hydrated form is exothermic, and this means the hypothetical formation of hydrated ACC from the dehydrated form would be endothermic. In other words, ACC dehydration is an irreversible process, with the dehydrated form more stable than the hydrated. This behavior is in contrast to the exothermic hydration (with respect to liquid water) of oxides to form oxyhydroxides (43, 44), and of dehydrated zeolites to form hydrated ones (45). The DSC measurements indicate that the vaporization of water from synthetic hydrated ACC is endothermic. The dehydration peak near 100 °C is diffuse in both DSC and TGA, a rough integration of DSC peak, normalized to the amount of water loss, suggests that the enthalpy of dehydration is roughly equal to the enthalpy of vaporization of liquid water at 100 °C (40.87 kJ/mol). This enthalpy value suggests that the initial dehydration is essentially loss of physisorbed water. Further loss of more strongly bound water and restructuring of ACC occurs up to the crystallization peak at 327 °C. This phenomenon implies that the structural reorganization during dehydration of ACC is exothermic enough to more than compensate for the endothermic removal of H_2O.

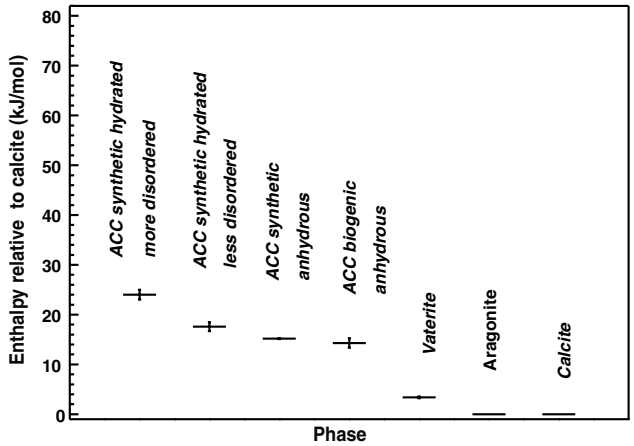

Fig. 2. Relative energetic stabilities of different calcium carbonate phases with respect to calcite. The enthalpy values of vaterite and aragonite are taken from (48) and (49) respectively.

Both hydrated and dehydrated ACC are much higher in enthalpy relative to bulk calcite than any of the crystalline polymorphs (aragonite, vaterite, or calcite). The major stabilization in enthalpy (energy) occurs during crystallization, and not during dehydration or during possible transformation among crystalline polymorphs.

Unlike synthetic ACC, biogenic ACC is almost anhydrous (0.25 mol of water), and is a transient phase which crystallizes easily to calcite. The crystallization enthalpy measured for the amorphous spicule samples at ambient conditions is $-14.3\pm$ 0.97 kJ/mol. This value is similar to that seen in the DSC measurement around 327 °C of dehydrated synthetic ACC material (-12.8 ± 0.5 to -15.4 ± 0.4 kJ/mol). This similarities in the enthalpy values suggests that the crystallization of anhydrous ACC from synthetic and biogenic sources takes place under different conditions with similar energetics. Nevertheless, the mechanism of crystallization may be different for synthetic and biogenic anhydrous ACC. The similarity of crystallization energetics for the synthetic Mg-free and biogenic Mg-containing samples also suggests that the effect of 5 mol% Mg in biogenic ACC on the enthalpy of crystallization is negligible.

Politi et al. (8) and Killian et al. (11) observed three spectroscopically distinct mineral phases in forming calcitic biominerals (from sea urchin spicules and teeth). The first phase (termed type 1) is rarely found, the second (type 2) is the most abundant phase observed during biomineral formation, and finally in the mature parts of the biominerals the only phase is biogenic calcite (type 3). By comparison with synthetic hydrated ACC and calcite, the authors identified the spectra of type 1 to correspond to hydrated ACC and type 3 to calcite. There was, however, no synthetic reference material to assign the spectrum of type 2. But the authors inferred that type 2 is anhydrous ACC. To our knowledge the present results show the full energetic characterization of anhydrous synthetic and biogenic ACC. The similarity of water contents and crystallization enthalpies of biogenic and dehydrated synthetic ACC strongly suggest that the majority of biogenic ACC is indeed anhydrous. This observation suggests a general trend in the development of spicules and likely other biominerals, where the freshly deposited material is composed of hydrated ACC, which rapidly transforms into a transient anhydrous phase, and finally to biogenic calcite (46).

The enthalpies of crystallization for various hydrous synthetic ACC samples were not constant. Instead two groups were observed: more metastable and less metastable hydrated phases. There was no correlation between the measured enthalpies and the water content or particle size. The only noticeable qualitative differences were found in the XRD patterns (see Fig. 1). We observed much lower intensity of the broad diffuse maxima in the XRD patterns of the samples with more exothermic crystallization enthalpies (more metastable hydrated ACC-1 and 2). The XRD results suggest that these samples are more disordered and contain less short-range order than those with less exothermic crystallization enthalpies (less metastable hydrated ACC-3 to 5). However these differences are difficult to quantify, most of the samples were consumed for calorimetry, and any leftover materials crystallized with aging.

If ACC is formed from aggregated prenucleation clusters, then the size of the cluster could determine the short-range order of the sample. Studies on calcium carbonate solutions indicate an initial size of approximately 0.6–1 nm, but after nucleation, 6 nm clusters were still observed in solution (34). Small variations in the temperature, mixing, filtration, and aging of the initial ACC material may affect the size and aggregation of the initial prenucleation clusters. The nature of such short-range ordering was not examined further in this study, but suggests an interesting topic for future investigations.

The enthalpies reported herein suggest that the crystallization of hydrous and anhydrous ACC to the other polymorphs (aragonite, vaterite) or to calcite is energetically downhill (see Fig. 2). The actual mechanisms of transformation along this energy landscape may not be straightforward since the possible role of prenucleation clusters, nanodomains, and reactions involving water make this system potentially very complex. One of these complex mechanisms, secondary nucleation, has recently been proposed for the crystallization and coorientation of biogenic-calcite nanoparticles (11). Our results clearly confirm that both synthetic and biogenic ACC are metastable phases with respect to crystalline forms of calcium carbonate, and that the major energy release comes with crystallization.

These results shed some light on the possible initial stages of crystallization of a calcium carbonate phase when CO_2 is injected underground. Near room temperature, rapid precipitation of ACC when a CO_2 plume encounters aqueous brine containing dissolved calcium appears likely, followed by the dehydration and transformations described above. At higher temperature and a more water-poor environment, the initial hydrous ACC phase may be bypassed, with the dehydrated form of ACC forming directly. The roles of temperature, salinity, and surface nucleation under such geologic conditions remain to be explored, but the energy landscape among phases developed by this study should provide useful constraints on possible reaction sequences.

Conclusions

To understand the crystallization pathway for ACC, the dehydration and crystallization enthalpies of ACC were measured using both DSC and isothermal solution calorimetry. Both hydrated and anhydrous ACC were found to be metastable with respect to crystalline forms. The dehydration of ACC is exothermic, implying that the structural reorganization during dehydration is exothermic enough to more than compensate for the endothermic release of H_2O and confirming that such dehydration is irreversible. The enthalpy of crystallization at ambient conditions for hydrated synthetic ACC ranges from -17 ± 1 to -24 ± 1 kJ/mol for several separately prepared samples. This variation may reflect differences in short-range order and/or nanodomain formation, with samples falling roughly into two groups: less ordered and more metastable vs. more ordered and less metastable. The enthalpy of crystallization of biogenic ACC at ambient conditions is -14.3 ± 0.97 kJ/mol, similar to that of dehydrated synthetic ACC around 327 °C (-12.8 ± 0.5 to -15.4 ± 0.4 kJ/mol for different samples). Previous studies in biogenic ACC inferred that the first phase formed is hydrated ACC, the second phase anhydrous ACC, and the final phase is calcite. The present data confirm that indeed the intermediate phase is anhydrous ACC, and that the transformations proceed through a sequence of phases of decreasing energetic metastability.

Materials and Methods

ACC samples were synthesized using previously reported methods (19, 20). A 0.02 M sodium carbonate solution was prepared by mixing 0.424 g of Na_2CO_3 (99.5%, Alfa Aesar) in 20 mL of 2 M NaOH solution (Alfa Aesar) and then diluting it to 200 mL with deionized water. A second solution containing 0.02 M calcium chloride was also prepared by dissolving 0.588 g of $CaCl_2{\cdot}2H_2O$ (99%, Alfa Aesar) in 200 mL of deionized water. Both these solutions were cooled in an ice bath for 6 h, then rapidly mixed with constant stirring and immediately filtered under vacuum. The precipitate was washed with acetone several times and vacuum dried overnight at 25 °C. All samples were equilibrated in the calorimetry suite, which is always maintained at ~24 °C and ~50% relative humidity, for 24 h before characterization and calorimetric measurements. The calcite sample was obtained from Fisher Chemicals (99.7%) and dried at 250 °C for 20 h.

Sea Urchin Spicules. Eggs of the California purple sea urchin, *S. purpuratus*, were fertilized and the embryos cultured at a concentration of 0.25% (egg volume/seawater volume) at 15 °C in filtered natural seawater according to the methods described by Foltz et al (47). Embryos were harvested for spicule isolation at prism stage (48 h postfertilization) and pluteus stage (72 h postfertilization). The spicules were extracted, cleaned from any external organic molecules, dried, and transported in dry ice. The dry spicules were analyzed within 24 h of extraction to avoid crystallization of ACC with aging. Detailed spicule preparation is described in the *SI Text*.

Powder X-ray Diffraction. The powder XRD patterns of the samples were collected using a Bruker AXS D8 Advance diffractometer (Bruker AXS, Inc.) with Cu K_α radiation source. Data were collected in the 2θ range of 10–120 ° with a step size of 0.01° 2θ and a collection time of 0.5–2 s/step using a zero-background sample holder. The XRD detection limit is approximately 2%–3%. In situ variable temperature powder XRD patterns of the samples were collected using an INEL X-ray diffractometer (INEL Inc.). The samples were heated from 110–500 °C in air at 10 °C/ min using the Symphonix software (Symphonix Devices). XRD patterns were collected in steps of 20 °C with a position sensitive detector covering 120° in 2θ using Co K_α radiation. The temperature of the heating stage furnace was calibrated using an Omega HH506R thermometer (OMEGA Engineering, Inc.) and the calibrated temperature range corresponds to 117–695 °C.

Solid-State Infrared Spectroscopy. The IR spectra of the samples were recorded by the KBr pellet technique using a Bruker Equinox 55 FTIR spectrometer (Bruker Optics Inc., range 400–4,000 cm^{-1}). A background spectrum with a pure KBr pellet was collected before each sample.

Thermogravimetric Analysis and Differential Scanning Calorimetry (TGA/DSC). TGA/DSC was carried out using a Netzsch STA 449 system (*NETZSCH*-Feinmahltechnik GmbH). The sample in a platinum crucible was heated from 25 °C–1,200 °C in argon at 10 °C/ min. A buoyancy correction was made. The water content was determined by the TGA weight loss curve. The DSC curves recorded simultaneously give the enthalpies associated with reactions such as dehydration, crystallization, and decomposition.

Surface Area Measurement. Surface area was measured by the BET method using a Micromeritics ASAP 2020 apparatus (*Micromeritics* Instrument Corporation). Five point isotherms in the P/P^o relative pressure range (P^o = saturation pressure) of 0.05-0.3 were measured by nitrogen adsorption at −196 °C. Each sample was vacuum degassed at room temperature for 18 h before the BET measurement.

SEM. SEM studies were carried out using a FEI XL30-SFEG high resolution Scanning Electron Microscope (FEI / Philips) without any additional coating of the sample. The microscope was operated at 1 kV because the ACC samples showed signs of beam damage at higher voltages. As the samples may have transformed and/or crystallized on aging before the SEM was done, but likely did not coarsen, we used the SEM mainly to confirm particle size (see *SI Text* for details).

Isothermal Acid Solution Calorimetry. A CSC 4400 isothermal microcalorimeter (Calorimetry Sciences Corporation) operated at 26 °C was used for the measurements of enthalpy of dissolution. Five milligrams of each sample was hand pressed into a pellet and dropped into a 5 N HCl solvent (~25 g) and taken in the calorimetric sample chamber. Mechanical stirring was used to aid dissolution. The calorimeter was calibrated by dissolving 15 mg pellets of KCl in water with stirring at 26 °C (see *SI Text* for details).

ACKNOWLEDGMENTS. We thank Fred Hayes (Materials Science Central Facilities, UC Davis) for the help with SEM. The early stages of this project were supported by DOE Grant DE-FG02-97ER-14749. The final stages were supported as part of the "Center of Nanoscale Control of Geologic CO_2," an Energy Frontier Research Center funded by the US Department of Energy, Office of Science, Office of Basic Energy Sciences under Award Number DE-AC02-05CH11231. The spicule work was supported by DOE Grant DE-FG02-07ER15899, and National Science Foundation (NSF) Grant CHE/BMAT—0613972 (to P.U.P.A.G.).

1. Mann S (1988) Molecular recognition in biomineralization. *Nature (London, United Kingdom)* 332:119–124.
2. Carlson WD (1983) Polymorphs of calcium carbonate and the aragonite-calcite transformation. *Rev Mineral* 11:191–225.
3. Addadi L, Raz S, Weiner S (2003) Taking advantage of disorder: amorphous calcium carbonate and its roles in biomineralization. *Adv Mater (Weinheim, Germany)* 15:959–970.
4. Weiner S, Levi-Kalisman Y, Raz S, Addadi L (2003) Biologically formed amorphous calcium carbonate. *Connect Tissue Res* 44(Suppl 1):214–218.
5. Weiss IM, Tuross N, Addadi L, Weiner S (2002) Mollusk larval shell formation: amorphous calcium carbonate is a precursor phase for aragonite. *J Exp Zool* 293:478–491.
6. Beniash E, Aizenberg J, Addadi L, Weiner S (1997) Amorphous calcium carbonate transforms into calcite during sea urchin larval spicule growth. *P Roy Soc B-Biol Sci* 264:461–465.
7. Politi Y, et al. (2006) Structural characterization of the transient amorphous calcium carbonate precursor phase in sea urchin embryos. *Adv Funct Mater* 16:1289–1298.
8. Politi Y, et al. (2008) Transformation mechanism of amorphous calcium carbonate into calcite in the sea urchin larval spicule. *Proc Natl Acad Sci USA* 105:17362–17366.
9. Aizenberg J, Lambert G, Weiner S, Addadi L (2002) Factors involved in the formation of amorphous and crystalline calcium carbonate: a study of an ascidian skeleton. *J Am Chem Soc* 124:32–39.
10. Aizenberg J, Ilan M, Weiner S, Addadi L (1996) Intracrystalline macromolecules are involved in the morphogenesis of calcitic sponge spicules. *Connect Tissue Res* 34:255–261.
11. Killian CE, et al. (2009) Mechanism of calcite co-orientation in the sea urchin tooth. *J Am Chem Soc* 131:18404–18409.
12. Politi Y, Arad T, Klein E, Weiner S, Addadi L (2004) Sea urchin spine calcite forms via a transient amorphous calcium carbonate phase. *Science (Washingto, DC, USA)* 306:1161–1164.
13. Wang D, Wallace AF, De Yoreo JJ, Dove PM (2009) Carboxylated molecules regulate magnesium content of amorphous calcium carbonates during calcification. *Proc Natl Acad Sci USA* 106:21511–21516.
14. Reddy MM, Nancollas GH (1976) The crystallization of calcium carbonate. IV. The effect of magnesium, strontium and sulfate ions. *J Cryst Growth* 35:33–38.
15. Donners JJJM, et al. (2000) Amorphous calcium carbonate stabilized by poly(propylene imine) dendrimers. *Chem Commun (Cambridge)* 1937–1938.
16. Dai L, Cheng X, Gower LB (2008) Transition bars during transformation of an amorphous calcium carbonate precursor. *Chem Mater* 20:6917–6928.
17. Li M, Mann S (2002) Emergent nanostructures: water-induced mesoscale transformation of surfactant-stabilized amorphous calcium carbonate nanoparticles in reverse microemulsions. *Adv Funct Mater* 12:773–779.
18. Koga N, Nakagoe Y, Tanaka H (1998) Crystallization of amorphous calcium carbonate. *Thermochim Acta* 318:239–244.
19. Koga N, Yamane Y (2008) Thermal behaviors of amorphous calcium carbonates prepared in aqueous and ethanol media. *J Therm Anal Calorim* 94:379–387.
20. Michel FM, et al. (2008) Structural characteristics of synthetic amorphous calcium carbonate. *Chem Mater* 20:4720–4728.
21. Benson SM, Cole DR (2008) CO_2 sequestration in deep sedimentary formations. *Elements (Chantilly VA U S)* 4:325–331.
22. Doughty C (2010) Investigation of CO_2 plume behavior for a large-scale pilot test of geologic carbon storage in a saline formation. *Transport in porous media* 82:49–76.
23. Hovorka SD, Doughty C, Benson SM, Pruess K, Knox PR (2004) The impact of geological heterogeneity on CO_2 storage in brine formations: a case study from the Texas Gulf Coast. *Geol Soc Spec Publ* 233(Geological Storage of Carbon Dioxide):147–163.
24. Kharaka YK, Cole DR, Thordsen JJ, Kakouros E, Nance HS (2006) Gas-water-rock interactions in sedimentary basins: CO_2 sequestration in the Frio Formation, Texas, USA. *J Geochem Explor* 89:183–186.
25. Ketzer JM, et al. (2009) Water-rock-CO_2 interactions in saline aquifers aimed for carbon dioxide storage: experimental and numerical modeling studies of the Rio Bonito Formation (Permian), southern Brazil. *Appl Geochem* 24:760–767.
26. Fernandez-Diaz L, Pina CM, Astilleros JM, Sanchez-Pastor N (2009) The carbonatation of gypsum: pathways and pseudomorph formation. *Am Mineral* 94:1223–1234.
27. Raz S, Hamilton PC, Wilt FH, Weiner S, Addadi L (2003) The transient phase of amorphous calcium carbonate in sea urchin larval spicules: the involvement of proteins and magnesium ions in its formation and stabilization. *Adv Funct Mater* 13:480–486.
28. Rodriguez-Blanco JD, Shaw S, Benning LG (2008) How to make "stable" ACC: protocol and preliminary structural characterization. *Mineral Mag* 72:283–286.
29. Quigley D, Rodger PM (2008) Free energy and structure of calcium carbonate nanoparticles during early stages of crystallization. *J Chem Phys* 128:221101-1–221101-4.
30. Tribello GA, Bruneval F, Liew CC, Parrinello M (2009) A molecular dynamics study of the early stages of calcium carbonate growth. *J Phys Chem B* 113:11680–11687.
31. Nebel H, Neumann M, Mayer C, Epple M (2008) On the structure of amorphous calcium carbonate—a detailed study by solid-state NMR spectroscopy. *Inorganic Chemistry (Washington, DC USA)* 47:7874–7879.
32. Levi-Kalisman Y, Raz S, Weiner S, Addadi L, Sagi I (2002) Structural differences between biogenic amorphous calcium carbonate phases using X-ray absorption spectroscopy. *Adv Funct Mater* 12:43–48.
33. Gebauer D, Voelkel A, Coelfen H (2008) Stable prenucleation calcium carbonate clusters. *Science (Washington, DC USA)* 322:1819–1822.
34. Pouget EM, et al. (2009) The initial stages of template-controlled $CaCO_3$ formation revealed by cryo-TEM. *Science (Washington, DC, USA)* 323:1455–1458.
35. De Yoreo JJ, et al. (2009) Rethinking classical crystal growth models through molecular scale insights: consequences of kink-limited kinetics. *Cryst Growth Des* 9:5135–5144.
36. Meldrum Fiona C, Colfen H (2008) Controlling mineral morphologies and structures in biological and synthetic systems. *Chem Rev* 108:4332–4432.
37. Wan P, et al. (2007) A novel approach to study the dynamic process of calcium carbonate crystal growth by microcalorimetric method. *Mater Sci Eng* A458:244–248.
38. Wolf G, Gunther C (2001) Thermophysical investigations of the polymorphous phases of calcium carbonate. *J Therm Anal Calorim* 65:687–698.
39. Pitcher MW, et al. (2005) Energy crossovers in nanocrystalline zirconia. *J Am Ceram Soc* 88:160–167.
40. Rimer JD, Trofymluk O, Navrotsky A, Lobo RF, Vlachos DG (2007) Kinetic and thermodynamic studies of silica nanoparticle dissolution. *Chem Mater* 19:4189–4197.
41. Asta M, Kauzlarich SM, Liu K, Navrotsky A, Osterloh FE (2007) Inorganic nanoparticles. Unique properties and novel applications. *Material Matters (Milwaukee, WI, USA)* 2:3–6.
42. Navrotsky A (2006) Calorimetry of nanoparticles, surfaces, interfaces, thin films, and multilayers. *J Chem Thermodyn* 39:2–9.
43. Navrotsky A, Mazeina L, Majzlan J (2008) Size-driven structural and thermodynamic complexity in iron oxides. *Science (Washington, DC, USA)* 319:1635–1638.
44. McHale JM, Auroux A, Perrotta AJ, Navrotsky A (1997) Surface energies and thermodynamic phase stability in nanocrystalline aluminas. *Science (Washington, DC, USA)* 277:788–791.
45. Navrotsky A, Trofymluk O, Levchenko AA (2009) Thermochemistry of microporous and mesoporous materials. *Chem Rev (Washington, DC, USA)* 109:3885–3902.
46. Politi Y, et al. (2008) Transformation mechanism of amorphous calcium carbonate into calcite in the sea urchin larval spicule. *Proc Nat'l Acad Sci USA* 105:17362–17366.
47. Foltz Kathy R, Adams Nikki L, Runft Linda L (2004) Echinoderm eggs and embryos: procurement and culture. *Methods Cell Biol* 74:39–74.
48. Wolf G, Konigsberger E, Schmidt HG, Konigsberger LC, Gamsjager H (2000) Thermodynamic aspects of the vaterite-calcite phase transition. *J Therm Anal Calorim* 60:463–472.
49. Wolf G, et al. (1996) Thermodynamics of $CaCO_3$ phase transitions. *J Therm Anal* 46:353–359.
50. Majzlan J, Navrotsky A, Schwertmann U (2004) Thermodynamics of iron oxides: Part III. Enthalpies of formation and stability of ferrihydrite (.apprx.$Fe(OH)_3$), schwertmannite (.apprx.$FeO(OH)_{3/4}(SO_4)_{1/8}$), and .vepsiln.-$Fe_2O_3$. *Geochim Cosmochim Ac* 68:1049–1059.